

Exploring the Relationship between Samples and Masks for Robust Defect Localization

Jiang Lin¹, Yaping Yan²,

¹PALM Lab, Southeast University

²PALM Lab, Southeast University

220215663@seu.edu.cn, yan@seu.edu.cn

Abstract

Defect detection aims to detect and localize regions out of the normal distribution. Previous approaches model normality and compare it with the input to identify defective regions, potentially limiting their generalizability. This paper proposes a one-stage framework that detects defective patterns directly without the modeling process. This ability is adopted through the joint efforts of three parties: a generative adversarial network (GAN), a newly proposed scaled pattern loss, and a dynamic masked cycle-consistent auxiliary network. Explicit information that could indicate the position of defects is intentionally excluded to avoid learning any direct mapping. Experimental results on the texture class of the challenging MVTec AD dataset show that the proposed method is 2.9% higher than the SOTA methods in F1-Score, while substantially outperforming SOTA methods in generalizability.

1 Introduction

Defect detection is a crucial and formidable task in industrial production and automation. Defects exhibit uncertain appearances, often appearing as small anomalies that are partially intermixed with normal regions. Additionally, the challenge of manual annotation limits the effectiveness of conventional visual inspection methods, leading recent approaches to adopt unsupervised techniques for addressing this task. In recent years, the rapid development of generative methods has led to the proposal of several reconstruction-based methods. Many methods employ Generative Adversarial Network (GAN) (Goodfellow et al. 2020) or Autoencoder (Bergmann et al. 2018) for image reconstruction, followed by anomaly level estimation through comparison of the input and reconstructed images. The aforementioned methods, however, suffer from imperfect reconstructions and noisy outputs resulting from suboptimal distance metrics. Despite attempts (Akçay, Atapour-Abarghouei, and Breckon 2018; Akçay, Atapour-Abarghouei, and Breckon 2019; Deng and Li 2022; Zavrtnik, Kristan, and Skočaj 2021a) to address these issues, they share a similar paradigm: identifying defects by modeling the normal distribution.

However, the training source may not provide sufficient data to adequately model normality, leading to imperfect reconstructions and all kinds of other issues. While referencing the normal distribution is crucial for anomaly detection in object classes, it becomes redundant for texture classes as defects can be discerned by examining the samples alone. Variations in environmental factors could also disrupt the distribution of normality, constituting difficulty for generalizing. The purpose of applying distance metrics is to identify the regions that have undergone certain modifications while being restored to the modeled normality, which no longer applies if normality also changes. We aim to optimize the reconstruction process by localizing the areas in need of reconstruction directly, rather than reconstructing them first and subsequently identifying which areas have been reconstructed. We commence by examining simple self-supervised methods and promptly discern that they may adopt shortcuts with a limited number of training samples. This has prompted us to adopt an innovative approach that eliminates all ground truth information in the learning process, thereby precluding any shortcuts.

Specifically, we employ a Generative Adversarial Network (GAN) to facilitate the transition between synthetic anomalies and arbitrary masks, while emphasizing that these two distributions are entirely independent. While the generator could fulfill the training objective by generating random masks, it is expected to produce annotations relevant to the input. Although the outputs initially conformed to our expectations, the network subsequently started generating arbitrary masks. However, there is an inherent correlation between the two distributions. In simple terms, the mask is characterized by a binary nature with distinct black and white markings. The generator must discern that the inputs also possess a binary nature, comprising both defective and normal regions. Subsequently, it can acquire the ability to associate negative areas with black labels and vice versa. To facilitate the exploration of the correlation between the two distributions, we propose a novel loss function called the scaled pattern loss. The proposed approach establishes a bidirectional pixel-wise mapping, thereby preventing the generator from producing arbitrary outputs. Additionally, we propose a dynamic masked cycle-consistent loss that incentivizes the network to accurately localize defects even in the absence of ground truth. Through the collaborative

efforts of these components, the network is capable of accurately identifying and matching appropriate markings to their corresponding areas in the input.

In contrast to previous approaches specifically designed for modeling normality distribution or discriminative learning mappings based on ground truth masks, our method is trained without explicit guidance to avoid leaking information that could indicate the location of defects and prevent overfitting. We provide unrelated masks solely just to ensure that the outputs resemble a mask while allowing the network to autonomously learn how to accurately localize defects. Our approach has successfully trained a model that operates seamlessly without the need for intermediate processes, showcasing robust generalization capabilities not only on test sets but also on additional test samples with diverse environmental variations. Experiments also suggest that the performance of our method is superior to the previous state-of-the-art methods while operating with no requirement for a threshold process before actual deployment. During the inference stage, our framework requires only one forward pass in the main generator, resulting in a twofold increase in operational speed compared to state-of-the-art methods.

Overall, our main contributions are listed as follows:

- We propose a unique solution that learns the ability to localize defects by searching for correlations between the sample distribution and the mask distribution.
- We propose a scaled pattern loss that enables a bidirectional pixel-wise mapping between the input and the output.
- We propose a dynamic masked cycle-consistent structure to implicitly optimize the localization results.

2 Related work

We briefly review previous literature on surface defect detection in this section. A primary difficulty in tackling this problem is the acquisition of defective samples. Because of this, recent researches mainly focus on unsupervised or self-supervised methods.

A great number of anomaly detection models adopted a reconstructive approach. Generative methods such as GAN (Schlegl et al. 2017, 2019) or autoencoders (Bergmann et al. 2018; Gong et al. 2019) enable powerful reconstruction ability using normal data only. Under the assumption that these models would not successfully recover the defects, the localization map is produced by the reconstruction error between the image and its reconstruction (Sakurada and Yairi 2014; Zavrtnik, Kristan, and Skočaj 2021b). Distance metrics such as l_2 distance (Hadsell, Chopra, and LeCun 2006) or SSIM (Bergmann et al. 2018) are used for better measurement. However, the models might be able to reconstruct defects as well though they were not present in training, leading to low error in the comparison and causing inaccurate localization results. In (Zavrtnik, Kristan, and Skočaj 2021a), a discriminative network is introduced to capture subtle differences between the inputs and the reconstructions. Some other works have tried to use memory-based autoencoders to further avoid defective reconstructions (Park, Noh, and Ham 2020).

Besides the over-generalization of defects, another issue is the unsatisfied reconstructions regarding normal regions, leading to inaccurate localization. Some methods seek ways to generate images of higher quality. Bergmann et al. apply structural similarity to autoencoders and improve the reconstruction quality. In (Deng and Li 2022), a trainable one-class bottleneck embedding module is designed to acquire more accurate reconstructions while excluding noises.

Due to the lack of defect samples, which is essential for the training process of a lot of frameworks, self-supervised methods are introduced to serve as a solution to the dire need for defect samples. Many methods (DeVries and Taylor 2017; Yun et al. 2019; Zhong et al. 2020) fabricate anomalies by replacing small rectangular regions of the original image with other values. (Li et al. 2021) propose the Cut-Paste augmentation to generate defect images by cutting a structural image patch from itself and randomly pasting them to other places. It highlights the need to synthesize samples close to the normal image distribution. Zavrtnik, Kristan, and Skočaj proposed an augmentation method by utilizing a Perlin noise mask to combine normal images with random image sources from (Cimpoi et al. 2014). The generated anomalies take various forms and contain both subtle and obvious defects.

These methods provide solid solutions for data augmentation. However, a gap exists between the distributions of the fabricated data and real-world defects. This results in generalization issues and severely impacts the performance of self-supervised methods. While the corrections provided by labels are proved to be useful in training, overfitting issues could occur at the same time.

3 Method

This paper proposes a novel unsupervised framework for defect localization in textures. Fig. 1 illustrates the overall structure of the proposed framework. The proposed method is mainly composed of a generator, a discriminator, and a dynamic masked cycle-consistent network with the ultimate purpose of training the main generator to conduct defect localization. The fundamental concept is to deliberately exclude any explicit information that could instruct the network on how to perform the task correctly. There are no self-supervised masks or anomaly scores provided as guidance, thereby allowing the network to learn how to localize an anomaly in textures rather than simply memorizing local appearances without considering the entire image. To train in the absence of real-world defective samples, we gain inspiration from the augmentation method proposed in (Zavrtnik, Kristan, and Skočaj 2021a) along with a newly proposed progressive opacity strategy to create the training samples.

3.1 Unpaired Transition

The GAN architecture is employed to facilitate the generator in acquiring the capability of seamlessly transforming the anomalous segment within an image into corresponding localization masks autonomously, without any explicit guidance. As shown in Fig. 1, the generator G is fed with defective samples, and its output M_o is discriminated against

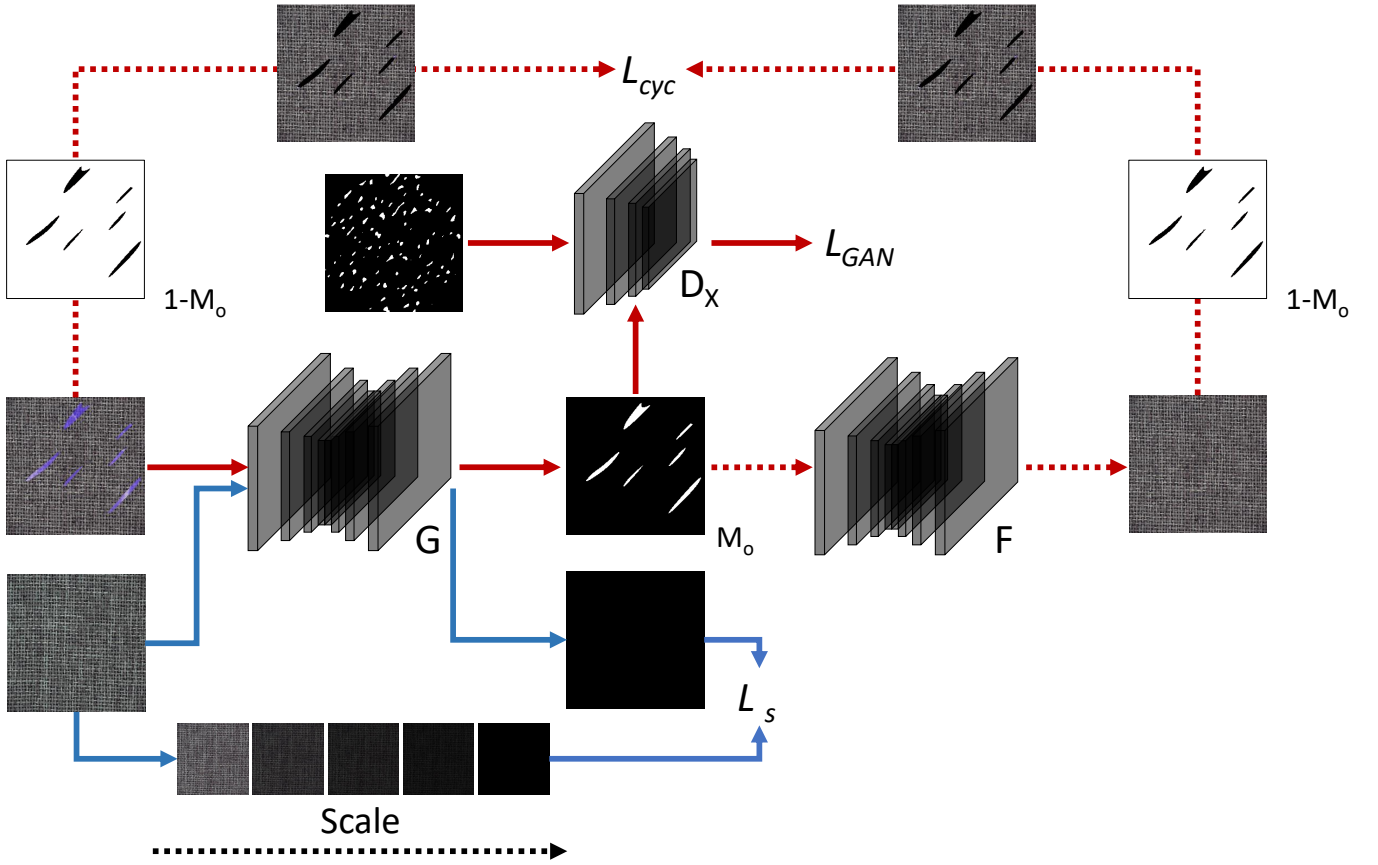


Figure 1: An overview of the proposed framework. D_Y is identical structured as D_X . It is not included in the graph for the overall visibility. In the training stage, the above components jointly train G to adopt the ability of defect detection. In the inference stage, we forward the inputs through G to acquire the localization results.

the mask samples by the discriminator D_Y . The objective is formulated as:

$$\mathcal{L}_{GAN}(G, D_Y, X, Y) = \mathbb{E}[\log(1 - D_Y(G(x)))] + \mathbb{E}[\log D_Y(y)], \quad (1)$$

where X and Y represent the domain of defective samples and pseudo labels respectively, and x and y are the images drawn from each domain.

Both X and Y are generated in Sec. 3.4, but they are not related which means y does not possess the correct information that localizes could localize defects in x . Therefore, after initially observing outputs related to the inputs, soon the generator starts to produce random masks. Numerous existing methods could potentially achieve a more precise transition. However, their usage of the corresponding ground truth cause information leak and subsequently lead to overfitting, which is undesirable in our study.

3.2 Scaled Pattern Loss

To build a connection between the inputs and the outputs, we proposed a new loss function termed the scaled pattern loss (SP loss). The goal of the SP loss is to create a pixel-wise bidirectional mapping between the input and the output

of the generator, preventing the generator from producing arbitrary localizations. To achieve that, we fed the network with normal samples, and expect the network to produce a linearly scaled version of the input which we named as the invisible pattern. The formula is shown below:

$$I_s = I_n \times \alpha - \beta \quad (2)$$

$$\mathcal{L}_S(I_p, I_s) = \|I_p - I_s\|_1, \quad (3)$$

where I_s is the scaled version of inputs and I_p is the output of the generator. Symbol α and β control the scale level of the image. Both of them are adjustable hyperparameters, and we recommend setting $\alpha = 0.005$ and $\beta = 0.995$.

The invisible pattern is imperceptible to the human eye, and its corresponding regions can be interpreted as negative predictions during inference. By jointly working with GAN, the proposed loss function effectively compels the generator to produce outputs that are closely aligned with the input. It also incorporates valuable information in the negative regions of the output, which can be utilized in the dynamic correction process.

3.3 Dynamic Correction

Despite the theoretical feasibility of the above structure, the training process is found to be volatile in practice. The adversarial loss and the scaled pattern loss tend to collide and often fail to coexist. As the training advance, one of them may become dominant and exclude the effect of the other. Inspired by previous works (Zhu et al. 2017), we proposed a dynamic mask cycle-consistent loss (DMCC) to ensure the generation of the scaled pattern and provide dynamic correction to the network.

A second generator F and a corresponding discriminator D_X are applied to recover the original image from the information preserved in the invisible pattern. This external demand for information, in turn, serves as a driving force for the proper generation of the invisible pattern, thereby enhancing the overall network stability. However, we observed a slight decline in performance and promptly recognized that this could be attributed to the unsuccessful recovery of defective areas. The presence of these regions hampers further reduction in loss and induces network turbulence, thereby gradually impeding optimal convergence during training. An effective approach is to utilize the mask that synthesizes the defect to eliminate the defective region during the calculation process of cycle-consistent loss. To avoid reliance on ground truth information, we employ the output from generator G as a filtering mask. In this manner, the turbulence originating from the defective region will gradually diminish as the localization accuracy improves, thereby establishing a positive feedback loop. This process is denoted as M and the objective can be formulated as:

$$\mathcal{L}_{cyc}(G, F) = \mathbb{E}[\|M(F(G(x))) - M(x)\|_1] + \mathbb{E}[\|G(F(y)) - y\|_1]. \quad (4)$$

To maintain the balance between the losses, we assign proper weight to each loss and the full objective is:

$$\begin{aligned} \mathcal{L}(G, F, D_X, D_Y) = & \mathcal{L}_{GAN}(G, D_Y, X, Y) \\ & + \mathcal{L}_{GAN}(F, D_X, Y, X) \\ & + \lambda_1 \mathcal{L}_{cyc}(G, F) \\ & + \lambda_2 \mathcal{L}_S(I_p, I_s). \end{aligned} \quad (5)$$

where λ_1 and λ_2 are set to 10 and 0.4 respectively, while considering adjustments based on the overall balance of the network.

3.4 Data Augmentation

In training, our method requires the presence of both defective and normal images. With only normal samples being accessible, augmentation methods could serve as an alternative to provide the defect samples needed. Therefore, we adopt the synthesis technique proposed by (Zavrtanik, Kristan, and Skočaj 2021a) to generate defective samples, while utilizing the Perlin noise mask generated during this process as pseudo labels. Note that, the pseudo labels and the defects are unaligned and randomly shuffled, which means no paired samples are utilized during training. Moreover, the final performance of the model is significantly influenced by the quality of simulated samples, given the absence of explicit information in training. Transparency plays a key role,

as models trained on obvious defects perform poorly on subtle ones. However, introducing more transparent defects may result in unstable training due to potential failure in perceiving defective areas within the training samples.

To address this issue, we propose a progressive opacity strategy (Pos) that gradually enhances transparency throughout the training process, ultimately yielding nearly imperceptible defects. Specifically, the training data is regenerated every 50 epochs based on the opacity value provided by Pos, allowing the model to achieve a stable state through the initial utilization of apparent defects. Subsequently, the model is further optimized to enhance its ability in distinguishing more subtle defects, while avoiding potential instability.

4 Experiments

The proposed method is benchmarked and compared with state-of-the-art defect detection methods in this section. Furthermore, the generalizability of our model is evaluated through simulations conducted in various environments.

4.1 Performance

The MVTEC anomaly detection dataset (Bergmann et al. 2019) consists of 5 texture classes and 10 object classes. Our proposed method is specifically designed for detecting texture defects, thus the 5 texture classes is utilized in the evaluation. AUROC is a commonly used metric that measures performance across all thresholds. However, in imbalanced problem settings, it tends to disregard false positives and excessively penalize false negatives. Localizations in defect detection should not be excessively ambiguous, as it is crucial to acknowledge that classification tasks already the presence of defects in specific regions. Methods with vague localization results often achieve an AUROC near 1 (the maximum value), while offering obvious deficiencies in their results as shown in Fig. 2. F1-Score is a metric that is specifically designed for imbalanced problem settings, making it a more suitable evaluation metric in the experiments below.

The images are resized to a predetermined resolution (256×256) and then normalized being fed into the network. The generator (He et al. 2016) and discriminator (Isola et al. 2017) adopt structures that are similar to previous methods (Zhu et al. 2017; Kim et al. 2019). The model is trained for 1000 epochs using a batch size of 1 on an RTX 3080 GPU. An Adam optimizer (Kingma and Ba 2014) with $\beta = (0.5, 0.999)$ is applied with a 0.0002 learning rate. The data augmentation method mentioned in Sec. 3.4 is utilized to generate a total of 300 simulated defective samples and masks for training.

The overall performance of our proposed method is compared with recent state-of-the-art approaches in Tab. 1, and the best results are highlighted in boldface. Our method surpasses the previous SOTA by **2.9%** in average and reaches a new SOTA of **68.9%** on F1-measure. The visual comparison with previous methods is shown in Fig. 2. Further analysis reveals that, apart from the statistical aspects, our method also yields results of superior visual quality. In contrast to vague localization, our model delivers more precise results

| Class | PaDim | CFlow | PatchCore | DRAEM | Ours |
|---------|-------|-------|-----------|-------------|-------------|
| Wood | 47.2 | 53.5 | 47.2 | 68.3 | 70.7 |
| Carpet | 58.1 | 63.6 | 59.8 | 50.5 | 66.1 |
| Tile | 53.9 | 66.8 | 63.6 | 91.3 | 86.2 |
| Leather | 49.5 | 55.4 | 45.0 | 63.5 | 66.4 |
| Grid | 32.9 | 32.4 | 18.5 | 56.8 | 55.8 |
| AVG | 48.3 | 54.3 | 46.8 | 66.0 | 68.9 |

Table 1: Results of anomaly localization on all textures in MVTec dataset(F1-Score) from PaDim (Defard et al. 2021), CFlow (Gudovskiy, Ishizaka, and Kozuka 2022), PatchCore (Roth et al. 2022), DRAEM (Zavrtanik, Kristan, and Skočaj 2021a) and our proposed method.

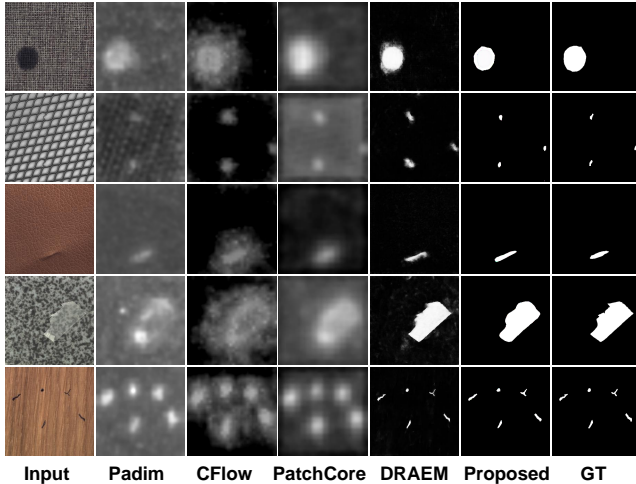


Figure 2: Comparison of anomaly maps (No threshold). The anomalous images and the ground truth are shown in the first and the last column. The middle five columns, from left to right, are results from PaDim(Defard et al. 2021), CFlow(Gudovskiy, Ishizaka, and Kozuka 2022), PatchCore(Roth et al. 2022), DRAEM(Zavrtanik, Kristan, and Skočaj 2021a), and our proposed method.

with less noise. The average prediction time of the previous SOTA method (Zavrtanik, Kristan, and Skočaj 2021a) is 0.013113 seconds, whereas our method achieves a prediction time of approximately 0.006001 seconds under the same test environment, making it twice as fast. Further details on the evaluation of inference speed and additional experiments conducted with additional datasets are provided in the supplementary material.

4.2 Generalizability

Previous approaches have demonstrated consistent advancements in achieving optimal performance. However, in addition to the issue of inappropriate evaluation metrics, insufficient attention has been given to the generalizability of a model. The assessment of the performance on unseen test scenarios is essential for determining the applicability of a model.

In this subsection, we conduct additional experiments in

simulated environments to evaluate the generalizability of our approach. Image attributes, such as Contrast, Brightness, and Hue are utilized to create a simulated illumination environment of two levels of settings. The general setting adjusts brightness and contrast, while the hard setting also varies hue to reflect different lighting conditions. The localization results in both settings are shown in Fig. 3. In the general setting, most methods experience some level of degeneration and significant performance drops occur in a few classes. When hue changes are introduced, the performance of previous methods drops more severely and most methods suffer from medium to extreme performance drops. The statistics presented in Tab. 2 demonstrate that our method is capable of maintaining consistent performance and surpassing others by **12.4%** and **18.3%** in the general and hard settings, respectively.

The performance of DRAEM (Zavrtanik, Kristan, and Skočaj 2021a), a reconstruction-based method, exhibited the most significant decrease. These methods heavily rely on modeling normal samples and face challenges in adapting to shifts in input distribution, such as variations in light or color, which ultimately leads to a significant decline in performance. A More detailed analysis is provided in the supplementary material. On the contrary, feature-based methods like CFlow (Gudovskiy et al., 2022), Padim (Defard et al., 2021), and PatchCore (Roth et al., 2022) are less affected by this issue as they can effectively model normality in a high-dimensional feature space. In this way, the network captures high-level feature information while paying less attention to details. However, the changes in the overall environment may also present challenges for the feature extraction process in these methods. Consequently, when applied to unseen test scenarios, we observed suboptimal performance on average and significant performance deteriorations in specific categories as shown in Tab. 2. In contrast to existing methods that rely on modeling the distribution of normal samples, our approach directly localizes defective regions upon the given samples. Since the training samples were not accompanied by any ground truth, the network avoids making assumptions about the input distribution, thereby demonstrating improved robustness in adapting to environmental variations. The performance of our method exhibits a certain decline, yet it maintains an acceptable level with an F1-Score of 59.7% in the general setting and 49.7% in the hard setting.

5 Ablation study

In this section, we perform an ablation analysis to investigate the individual contributions of each module and the impacts of the pos strategy, which is essential for comprehending our framework as it integrates components with distinct objectives.

5.1 Architecture

The components are reassembled to conduct an ablation study to effectively demonstrate the impact of individual elements. The components are: (i) GAN uses only the basic GAN structure with an identical simulated data source as

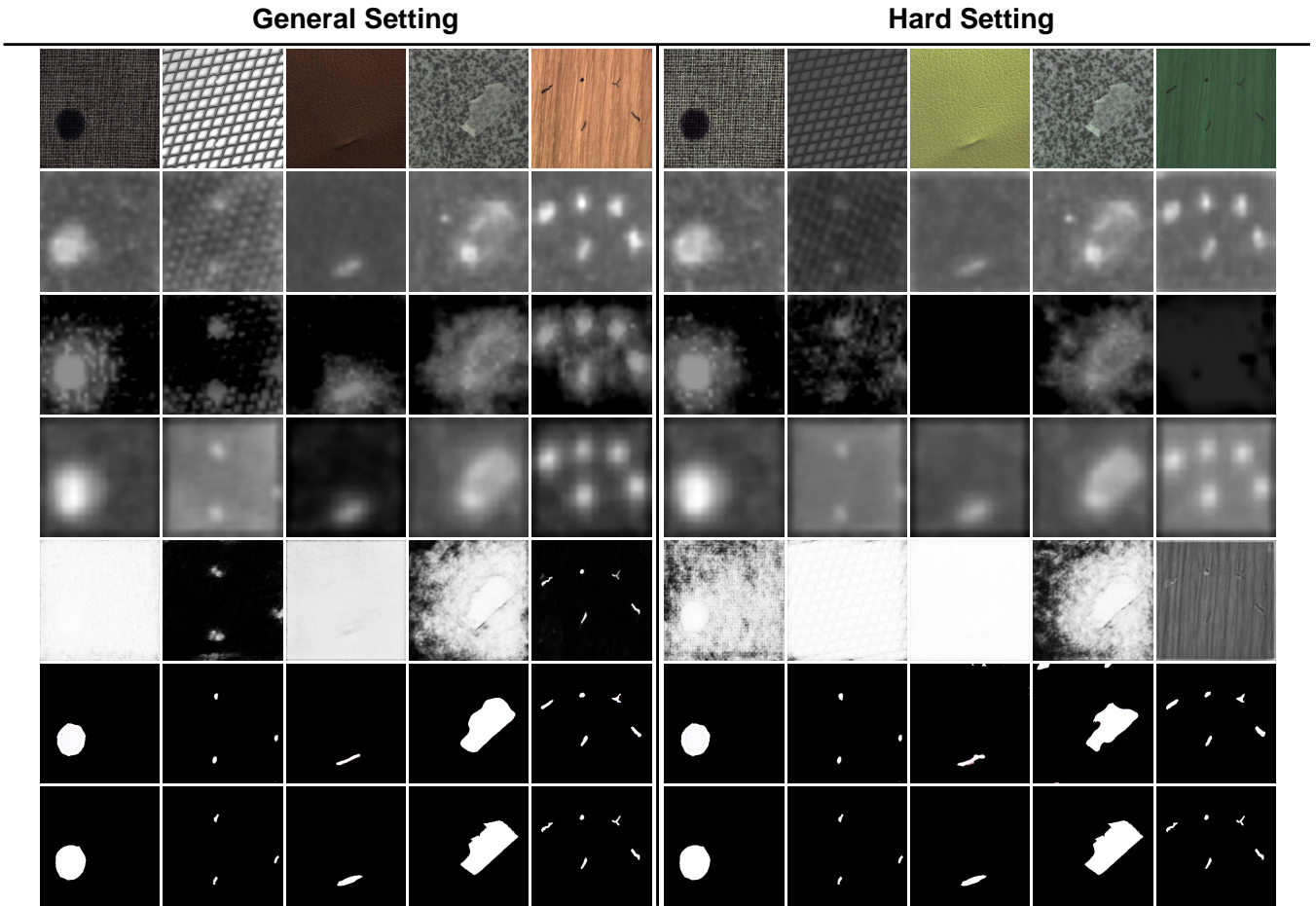


Figure 3: Visual results compare anomaly localization methods’ generalization ability. The test source consisting of the general setting (left) and the hard setting (right) is shown in the first row. The ground truth is at the bottom of the figure. The middle five rows show the localization results from PaDim (Defard et al. 2021), CFlow (Gudovskiy, Ishizaka, and Kozuka 2022), PatchCore (Roth et al. 2022), DRAEM (Zavrtanik, Kristan, and Skočaj 2021a) and the implementation of our proposed method respectively.

the others. (ii) Scaled denotes the scaled pattern loss while introducing another stream of normal inputs. (iii) Cyc is the auxiliary network with an additional generator and discriminator, enabling cycle-consistent loss. (iv) Mask is the dynamic mask we enforce on the Cyc to reduce turbulence in the loss. (v) Pos is the progressive opacity strategy that we applied to data generation. A combination of initials such as G.S.C represents the setting where the corresponding components are enabled, and the content within the parenthesis indicates the opacity setting.

Tab. 3 reports that G.S.C.M(Pos) demonstrates superior performance compared to others, while the G which is the simplest form of the network produces a result of only 2.8%. After a closer inspection, the table reveals a general increasing trend as each component is added. The G.S and G.C.M have increased by 34.4% and 24.6% respectively compared to the G. However, contrary to this overall trend, the G.S.C shows performance deterioration with the additional Cyc component. Sec. 3.3 briefly discusses the possible cause for this behavior and proposes the corresponding solution we

denoted as the Mask.

Generally, simple G is not capable of performing the defect detection task. Both the SP loss and DMCC loss significantly contribute to the final performance, with their combined effort further enhancing the performance of the proposed framework. The SP loss relies on the DMCC loss to achieve stable training, while the DMCC loss requires the presence of the invisible pattern to conduct dynamic correction correctly.

5.2 Data Source

In our framework, we train the model to autonomously recognize and localize the defects in the adversarial process. The opacity value significantly influences the visibility of defects and plays a crucial role in determining the level of difficulty in recognizing them, thus making it a pivotal factor that affects the final performance. Therefore, we conduct extensive experiments to reveal how opacity setting affects the training.

As illustrated before, a progressive opacity strategy is

| Class | General Setting | | | | | Hard Setting | | | | |
|---------|-----------------|-------|-----------|-------|-------------|--------------|-------|-----------|-------|-------------|
| | PaDim | CFlow | PatchCore | DRAEM | Ours | PaDim | CFlow | PatchCore | DRAEM | Ours |
| Wood | 42.2 | 46.7 | 44.1 | 11.9 | 62.7 | 24.1 | 3.8 | 14.2 | 7.8 | 50.0 |
| Carpet | 36.4 | 56.0 | 51.2 | 5.3 | 63.2 | 44.4 | 51.6 | 52.3 | 3.5 | 57.2 |
| Tile | 44.9 | 54.5 | 61.3 | 15.7 | 75.4 | 41.5 | 54.6 | 55.6 | 14.3 | 63.5 |
| Leather | 49.3 | 47.8 | 44.9 | 1.6 | 49.8 | 23.6 | 9.3 | 19.3 | 1.3 | 29.9 |
| Grid | 14.4 | 31.5 | 7.3 | 2.4 | 47.7 | 23.6 | 31.2 | 8.9 | 2.0 | 48.2 |
| AVG | 37.4 | 47.3 | 41.8 | 7.4 | 59.7 | 31.4 | 30.1 | 30.1 | 5.8 | 49.7 |

Table 2: Results for generalization experiments under general setting (left) and hard setting (right) on PaDim (Defard et al. 2021), CFlow (Gudovskiy, Ishizaka, and Kozuka 2022), PatchCore (Roth et al. 2022), DRAEM (Zavrtanik, Kristan, and Skočaj 2021a) and our proposed method.

| Method | Architecture | | | | Opacity | | | | | AVG |
|--------------|--------------|--------|-----|------|---------|--------|--------|------------|-----|-------------|
| | GAN | Scaled | Cyc | Mask | 0(0.1) | 0(0.5) | 0(0.9) | O(0.1-0.9) | Pos | |
| G | ✓ | | | | | | | ✓ | | 2.8 |
| G.S | ✓ | ✓ | | | | | | ✓ | | 37.2 |
| G.C.M | ✓ | | ✓ | | | | | ✓ | | 27.4 |
| G.S.C | ✓ | ✓ | ✓ | | | | | ✓ | | 35.4 |
| G.S.C.M | ✓ | ✓ | ✓ | ✓ | | | | ✓ | | 51.1 |
| G.S.C.M(0.1) | ✓ | ✓ | ✓ | ✓ | ✓ | | | | | 15.9 |
| G.S.C.M(0.5) | ✓ | ✓ | ✓ | ✓ | | ✓ | | | | 40.4 |
| G.S.C.M(0.9) | ✓ | ✓ | ✓ | ✓ | | | ✓ | | | 30.9 |
| G.S.C.M(Pos) | ✓ | ✓ | ✓ | ✓ | | | | | ✓ | 68.9 |

Table 3: Anomaly localization results of ablation study on architecture (left) and opacity (right).

adopted to aid the training procedure. To verify the effectiveness of this strategy, we use fixed opacity 0.1, 0.5, and 0.9 as the control group. As depicted in Tab. 3, a deterioration in performance is initially observed with decreasing opacity of the training source, owing to the instability induced by high transparency training samples. The presence of more transparent defects, as discussed in Sec. 3.4, compels the model to discern subtle differences. However, identifying highly transparent simulated defects in the initial training phase can be challenging, which may cause confusion and disruption leading to network instability. The progressive opacity strategy (Pos) proposed in Sec. 3.4 aims to address this issue.

The impact of Pos on the network was investigated by conducting model training with varying opacity settings. G.S.C.M(0.1) delivers an unstable result of 15.9% in Tab. 3 and suffers from a high likelihood to collapse in training. The G.S.C.M(0.1) produces an unstable result of 15.9% in Tab. 3 and tends to collapse during training. Models trained with a 0.5 opacity value outperform those trained with 0.9, while also being capable of detecting more subtle defects. Pos facilitates early training by introducing obvious defects and then gradually increasing the transparency of synthetic defects to promote recognition of subtle issues. Experimental results have demonstrated its effectiveness, with a performance of **68.9%**, significantly outperforming other models trained under the same architecture but with different opacity settings.

We could conclude that the quality of the simulated data

has a huge impact on the final performance of the model. The structure of our model also allows training using unlabeled real-world defects. It is speculated that the accessibility to real-world defects may lead to improved convergence of the model. The supplementary material presents additional experimental results that compare models trained with varying opacity settings on a simulated test set of defects generated with different transparency levels.

6 Conclusion

In this paper, we pointed out that over-reliance on nominal data may hinder the applicability of defect localization methods. Our hypothesis posits that by removing explicit guidance during the training process, the model can develop the ability to discern relative defects in specific textures rather than solely acquiring superficial models that are heavily dependent on particular appearances learned during training. We proposed a new GAN-based framework that incorporates various constraints and implicit guidance to effectively localize defects. Notably, the trained model successfully identifies defects without relying on modeling nominal sample subspaces. The proposed method attains state-of-the-art performance on the benchmark datasets, while additional experiments substantiate its robust generalizability and superior inference efficiency. The potential of our framework can be further enhanced by leveraging raw defect samples from real-world scenarios to improve its performance, a practice uncommon in other methods that typically rely on

defective samples accompanied by ground truth information during training.

References

- Akçay, S.; Atapour-Abarghouei, A.; and Breckon, T. P. 2018. Ganomaly: Semi-supervised anomaly detection via adversarial training. In *Asian conference on computer vision*, 622–637. Springer.
- Akçay, S.; Atapour-Abarghouei, A.; and Breckon, T. P. 2019. Skip-ganomaly: Skip connected and adversarially trained encoder-decoder anomaly detection. In *2019 International Joint Conference on Neural Networks (IJCNN)*, 1–8. IEEE.
- Bergmann, P.; Fauser, M.; Sattlegger, D.; and Steger, C. 2019. MVTec AD—A comprehensive real-world dataset for unsupervised anomaly detection. In *Proceedings of the IEEE/CVF conference on computer vision and pattern recognition*, 9592–9600.
- Bergmann, P.; Löwe, S.; Fauser, M.; Sattlegger, D.; and Steger, C. 2018. Improving unsupervised defect segmentation by applying structural similarity to autoencoders. *arXiv preprint arXiv:1807.02011*.
- Cimpoi, M.; Maji, S.; Kokkinos, I.; Mohamed, S.; and Vedaldi, A. 2014. Describing textures in the wild. In *Proceedings of the IEEE conference on computer vision and pattern recognition*, 3606–3613.
- Defard, T.; Setkov, A.; Loesch, A.; and Audigier, R. 2021. Padim: a patch distribution modeling framework for anomaly detection and localization. In *International Conference on Pattern Recognition*, 475–489. Springer.
- Deng, H.; and Li, X. 2022. Anomaly Detection via Reverse Distillation from One-Class Embedding. In *Proceedings of the IEEE/CVF Conference on Computer Vision and Pattern Recognition*, 9737–9746.
- DeVries, T.; and Taylor, G. W. 2017. Improved regularization of convolutional neural networks with cutout. *arXiv preprint arXiv:1708.04552*.
- Gong, D.; Liu, L.; Le, V.; Saha, B.; Mansour, M. R.; Venkatesh, S.; and Hengel, A. v. d. 2019. Memorizing normality to detect anomaly: Memory-augmented deep autoencoder for unsupervised anomaly detection. In *Proceedings of the IEEE/CVF International Conference on Computer Vision*, 1705–1714.
- Goodfellow, I.; Pouget-Abadie, J.; Mirza, M.; Xu, B.; Warde-Farley, D.; Ozair, S.; Courville, A.; and Bengio, Y. 2020. Generative adversarial networks. *Communications of the ACM*, 63(11): 139–144.
- Gudovskiy, D.; Ishizaka, S.; and Kozuka, K. 2022. Cflowad: Real-time unsupervised anomaly detection with localization via conditional normalizing flows. In *Proceedings of the IEEE/CVF Winter Conference on Applications of Computer Vision*, 98–107.
- Hadsell, R.; Chopra, S.; and LeCun, Y. 2006. Dimensionality reduction by learning an invariant mapping. In *2006 IEEE Computer Society Conference on Computer Vision and Pattern Recognition (CVPR'06)*, volume 2, 1735–1742. IEEE.
- He, K.; Zhang, X.; Ren, S.; and Sun, J. 2016. Deep residual learning for image recognition. In *Proceedings of the IEEE conference on computer vision and pattern recognition*, 770–778.
- Isola, P.; Zhu, J.-Y.; Zhou, T.; and Efros, A. A. 2017. Image-to-image translation with conditional adversarial networks. In *Proceedings of the IEEE conference on computer vision and pattern recognition*, 1125–1134.
- Kim, J.; Kim, M.; Kang, H.; and Lee, K. 2019. U-gat-it: Unsupervised generative attentional networks with adaptive layer-instance normalization for image-to-image translation. *arXiv preprint arXiv:1907.10830*.
- Kingma, D. P.; and Ba, J. 2014. Adam: A method for stochastic optimization. *arXiv preprint arXiv:1412.6980*.
- Li, C.-L.; Sohn, K.; Yoon, J.; and Pfister, T. 2021. Cutpaste: Self-supervised learning for anomaly detection and localization. In *Proceedings of the IEEE/CVF Conference on Computer Vision and Pattern Recognition*, 9664–9674.
- Park, H.; Noh, J.; and Ham, B. 2020. Learning memory-guided normality for anomaly detection. In *Proceedings of the IEEE/CVF Conference on Computer Vision and Pattern Recognition*, 14372–14381.
- Roth, K.; Pemula, L.; Zepeda, J.; Schölkopf, B.; Brox, T.; and Gehler, P. 2022. Towards total recall in industrial anomaly detection. In *Proceedings of the IEEE/CVF Conference on Computer Vision and Pattern Recognition*, 14318–14328.
- Sakurada, M.; and Yairi, T. 2014. Anomaly detection using autoencoders with nonlinear dimensionality reduction. In *Proceedings of the MLSDA 2014 2nd workshop on machine learning for sensory data analysis*, 4–11.
- Schlegl, T.; Seeböck, P.; Waldstein, S. M.; Langs, G.; and Schmidt-Erfurth, U. 2019. f-AnoGAN: Fast unsupervised anomaly detection with generative adversarial networks. *Medical image analysis*, 54: 30–44.
- Schlegl, T.; Seeböck, P.; Waldstein, S. M.; Schmidt-Erfurth, U.; and Langs, G. 2017. Unsupervised anomaly detection with generative adversarial networks to guide marker discovery. In *International conference on information processing in medical imaging*, 146–157. Springer.
- Yun, S.; Han, D.; Oh, S. J.; Chun, S.; Choe, J.; and Yoo, Y. 2019. Cutmix: Regularization strategy to train strong classifiers with localizable features. In *Proceedings of the IEEE/CVF international conference on computer vision*, 6023–6032.
- Zavrtanik, V.; Kristan, M.; and Skočaj, D. 2021a. Draem—a discriminatively trained reconstruction embedding for surface anomaly detection. In *Proceedings of the IEEE/CVF International Conference on Computer Vision*, 8330–8339.
- Zavrtanik, V.; Kristan, M.; and Skočaj, D. 2021b. Reconstruction by inpainting for visual anomaly detection. *Pattern Recognition*, 112: 107706.
- Zhong, Z.; Zheng, L.; Kang, G.; Li, S.; and Yang, Y. 2020. Random erasing data augmentation. In *Proceedings of the AAAI conference on artificial intelligence*, volume 34, 13001–13008.

Zhu, J.-Y.; Park, T.; Isola, P.; and Efros, A. A. 2017. Unpaired image-to-image translation using cycle-consistent adversarial networks. In *Proceedings of the IEEE international conference on computer vision*, 2223–2232.